ADBA Computer Science
Cutting-Edge Scientific Solutions

e-ISSN: 3023-8544
RESEARCH ARTICLE
Vol.3 / No.1 / 2026 / pp.26-36
https://doi.org/10.69882/adba.cs.2026015

Dynamics, Stability, and Bifurcation in Discrete-Time Predator-Prey Model

Ansar Abbas *,1 **and Abdul Khaliq** *,2
*Department of Mathematics, Riphah International University, Lahore Campus, Pakistan.

ABSTRACT A discrete-time three-species food chain model is presented in this paper, focusing on bifurcation dynamics and chaos control. The transcritical and Neimark-Sacker bifurcations at distinct equilibrium points under specific parameter conditions are revealed by bifurcation and stability theory. Stabilizing chaotic dynamics is achieved using the Ott-Grebogi-Yorke (OGY) method. The dynamical behavior of the model is investigated by comparing phase portraits and time series across varying initial conditions. An assessment of stability is made, a topological classification is performed, and attractors are identified. Lyapunov exponent analysis also provides a deeper understanding of the system's complex behavior. In food chain models based on population, numerical simulations verify theoretical results by revealing the complex interplay among bifurcations, chaos, and control mechanisms.

KEYWORDS
Modeling FCM
Bifurcation
Topological classification
Chaos control
Maximum lyapunov exponent
Time series

INTRODUCTION

Ecosystems include predator-prey interactions, including predation and prey hunting. Numerous scholars have criticized the predator-prey model since Voltera and Lotka brought it into existence in the late 19th century (May 1974; Skalski and Gilliam 2001; Alarifi 2012). A deeper understanding of the original model is being conducted by scholars in order to make it more practical. It takes several factors into consideration, such as the time delay, the functional response, diffusion, etc. System stability and persistence have been demonstrated to be associated with positive periodic solutions. The Lotka-Voltera model describes the interactions between predators and prey. Lotka and Voltera developed the model independently in (Lotka 1925; Volterra 1962). The Hastings and Powell food chain model with three species is applied in (Khan *et al.* 2015) to harvest their control strategy for chaotic population growth.

$$\left.\begin{aligned} \frac{dx_1}{d\tilde{t}} &= Rx_1(1-\tfrac{x_1}{K}) - \tilde{c}_1\,\tilde{f}_{11}(x_1)x_2 \\ \frac{dx_2}{d\tilde{t}} &= \tilde{f}_{11}(x_1)x_2 - \tilde{f}_{12}(x_2)x_3 - \tilde{d}_1(x_2) \\ \frac{dx_3}{d\tilde{t}} &= \tilde{c}_2\tilde{f}_{12}(x_2)x_3 - \tilde{d}_2(x_3) \end{aligned}\right\} \tag{1}$$

Manuscript received: 23 November 2025,
Revised: 24 December 2025,
Accepted: 25 December 2025.

[1]kute_ansar@yahoo.com (**Corresponding author**).
[2]khaliqsyed@gmail.com

where $\tilde{f}_{1_j}(\tilde{V}) = \frac{\tilde{m}_j\tilde{V}}{\tilde{n}_j+\tilde{V}}, j = 1, 2.$

Various behaviors are included in this model, including steady state, limit cycle, period-2, and period-4. Threshold harvesting is incredibly helpful in conserving species and managing fisheries efficiently. Panday *et al.* (2018) proposes a three-species FCM in which capital costs of top predators suppress middle predators' growth rates, while middle predators' capital costs suppress prey growth rates.

$$\left.\begin{aligned} \frac{d\tilde{x_1}}{dt} &= \tilde{R_1}\tilde{x_1}(1-\tfrac{\tilde{x_1}}{K}) - \tfrac{\tilde{m}_1\tilde{A}_1\tilde{x_1}\tilde{x_2}}{\tilde{B}_1+\tilde{x_1}} \\ \frac{d\tilde{x_2}}{dt} &= \tfrac{\tilde{A}_1\tilde{x_1}\tilde{x_2}}{\tilde{B}_1+\tilde{x_1}} - \tfrac{\tilde{A}_2\tilde{x_2}\tilde{x_3}}{\tilde{B}_2+\tilde{x_2}} - d_1\tilde{x_2} \\ \frac{d\tilde{x_3}}{dt} &= \tfrac{\tilde{m}_2\tilde{A}_2\tilde{x_2}\tilde{x_3}}{\tilde{B}_2+\tilde{x_1}} - d_2\tilde{x_3} \end{aligned}\right\} \tag{2}$$

Chaotic conditions are investigated by using a Poincare section and the MLE in the system (2).

A positive correlation exists between population density and individual fitness in population biology, the Allee effect. A simulation of the Allee effect is provided in (Parshad *et al.* 2016). Based on their study, the following systems are globally attractive:

$$\left.\begin{aligned} \frac{\partial \tilde{u}}{\partial \tilde{t}} &= c_1\,\Delta\tilde{u} + \tilde{u} - \tilde{u}^2 - b_1\frac{\tilde{u}\tilde{v}}{\tilde{u}+\tilde{v}} \\ \frac{\partial \tilde{v}}{\partial \tilde{t}} &= c_2\,\Delta\tilde{v} - d_2\tilde{v} + b_2\frac{\tilde{u}\tilde{v}}{\tilde{u}+\tilde{v}} - b_3\frac{\tilde{v}\tilde{r}}{\tilde{v}+\tilde{r}} \\ \frac{\partial \tilde{r}}{\partial \tilde{t}} &= c_3\,\Delta\tilde{r} + \tilde{r}\,(\tilde{r}-\tilde{m})(k - \frac{b_4\tilde{r}}{\tilde{v}+c_3}) \end{aligned}\right\} \quad (3)$$

A considerable amount of research has been conducted on continuous models. Some species, especially those that grow rapidly, are better modeled as discrete populations for a variety of reasons. Species like these can be small and have short life cycles, as well as having no crossing between sexes. In comparison with continuous models, discrete-time models analyze dynamic behavior more effectively. Changes in parameters may cause a discrete system to exhibit more bifurcation and other dynamic behavior. Computer simulations and chaos control strategies are more effective with a discrete model.

The dynamic performance of discrete ecosystems has attracted more and more research attention in recent years (Ivanchikov and Nedorezov 2012; Baydemir *et al.* 2020; Jiang *et al.* 2020; Zhang *et al.* 2010). An integrative model of predator-prey interactions with parasites is discussed in (Selvam *et al.* 2020).

$$\left.\begin{aligned} s_{n+1} &= s_n + c\,[s_n(1-\tfrac{s_n}{a}) - s_n(s_n+v_v) - b\,s_n v_n] \\ t_{n+1} &= t_n + c\,[\tfrac{b\,\Theta}{k}s_n v_n - h t_n - \Theta t_n(u_n+v_v)] \\ u_{n+1} &= u_n + c\,[s_n u_n - t_n u_n - e u_n] \\ v_{n+1} &= v_n + c\,[t_n u_n - (e+d)v_n] \end{aligned}\right\} \quad (4)$$

The system (4) exhibits Neimark-Sacker bifurcation when the fixed point is positive. Dynamic chaos occurs when bifurcation parameters change. System chaotic motion is controlled by hybrid control methods.

A new chaos control strategy was proposed by (Ott *et al.* 1990). The method doesn't involve using existing dynamic control strategies or destroying the conditions that cause chaotic motion. In Romeiras *et al.* (1992) improve it even further. Time-delayed feedback control was introduced by Lithuanian physicist (Pyragas 1992). Research on chaos control and synchronization exploded over the next ten years, making it a hot spot in chaos. It has been proposed that linear state feedback control Holyst and Urbanowicz (2000) can be categorized into three types: sliding mode control (Chen and Chen 2007), adaptive Lyapunov control (Alasty and Salarieh 2007) and bioeconomic optimal control and bioeconomic optimal control (Chakraborty and Kar 2012) for predator-prey stability. A growing interest has been developed in studying chaos control in biological systems. A few authors have pointed out in (Din 2017; Abbas and Khaliq 2023; Gomes *et al.* 2006) that these chaos control methods have a nontrivial evolutionary significance. A control can also be modified by changing its properties or its fixed point. Chaos control in OGY utilizes small changes in parameters in real-time in order to maintain the original characteristics. Using the OGY approach, Feng (2020a,b) tested the Hassell and Ricker-type recruitment model. Both chaos and chaos control have been studied a lot. Research results in Vaseghi *et al.* (2017); Mobayen *et al.* (2018); Vaseghi *et al.* (2020) have been really valuable.

Continuous-time systems are discretized using Euler's method. This study investigates Transcritical and Neimark-Sacker bifurcations and controls the system with the OGY method. Recent studies Znegui *et al.* (2020a,b, 2021) have applied Poincare maps with analytical expressions to control chaos. The OGY method has enabled chaos computation (Pyragas 1995; Paine 1966).

In this work, the predator species impacts the prey's growth, leading to chaotic dynamics when $\alpha = 2.85$, $\beta = 3.14$, and $\rho = 2.54$. The focus is on controlling these chaotic behaviors, with instabilities observed at period-1 orbits. The relationship between control adjustments and timing is explored in model (5).

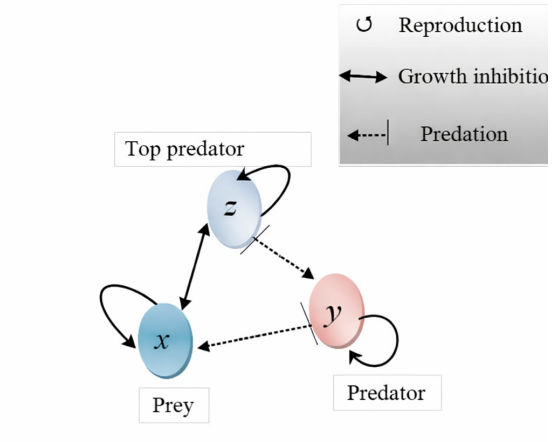

Figure 1 Dynamics of prey, predator, and top predator populations. Ecological interactions in Map (5) include predation (single dashed arrow), competition (double arrows), and reproduction (closed loops).

The paper is structured to systematically explore the dynamics and control of system (5). Section- *Modeling Equilibrium and Dynamics* provides a comprehensive topological classification of the system's equilibrium points, including the identification of fixed points and an analysis of their stability through linearization and eigenvalue evaluation. Section -*Transcritical Bifurcation Analysis at* EP_2 examines the transcritical bifurcation at EP_2, highlighting local qualitative shifts in system dynamics. Section -*Analyze Neimark-Sacker Bifurcation at* EP_5 presents the Neimark-Sacker bifurcation, establishing a rigorous theoretical framework and identifying the bifurcation parameters that govern the emergence of quasi-periodic dynamics.

Section -*Numerical Analysis* is dedicated to numerical simulations, which elucidate a variety of complex phenomena, including chaotic attractors, bifurcation diagrams, and the calculation of the maximum Lyapunov exponent. This section further provides a comparative analysis of phase portraits and time series under diverse initial conditions and parameter regimes, with the results systematically summarized in Tables 3 and 4. These findings reveal transitions among stable periodic orbits,quasi-periodic orbits, chaotic attractors, and stable limit cycles. In Section -*Stabilizing Three-Species Interactions*, the Ott-Grebogi-Yorke (OGY) control method is employed to stabilize an unstable fixed point, underscoring the practical applicability of chaos control strategies. Finally, Section -*Conclusion* concludes the paper by synthesizing the principal results and outlining prospective directions for future research.

MODELING EQUILIBRIUM AND DYNAMICS

Based on the three-species food chain in Figure 1, the following nonlinear difference equation model is developed:

$$\begin{pmatrix} x_{n+1} \\ y_{n+1} \\ z_{n+1} \end{pmatrix} = T \begin{pmatrix} x_n \\ y_n \\ z_n \end{pmatrix},$$

where

$$T(x,y,z) = \begin{pmatrix} \alpha x(1-x) - \beta xy \\ \gamma xy(x-z) \\ \rho yz \end{pmatrix}. \quad (5)$$

This model represents three distinct insect species. The system involves four positive parameters: α, β, γ, and ρ. The biological interpretation of these parameters is summarized in Table 1.

Table 1 Biological Meaning of Parameters

Param.	Meaning	Interpretation
α	Growth rate of prey x	Reproduction rate of species x without predators, limited by resources.
β	Predation rate of y on x	How strongly predator y feeds on prey x.
γ	Conversion efficiency	How effectively y converts consumed x into its own growth.
ρ	Predation of z on y	Impact of predator z feeding on y for its growth.

Furthermore, when there are no predators, the prey species grow naturally and reproduce on their own. However, when prey are hunted by predators (y), their reproduction decreases. It's important to understand that the term γ refers to the growth of predators (x) due to their consumption of prey species (y), and similarly for the prey. When predator (z) eats species (y), it leads to a growth rate ρ for predator (z). The hypothesis also suggests that species (y) and (z) interfere with species (x), but species (y) is mainly responsible for the higher reproduction rate of species (z). For determining the equilibrium and dynamic of a system, we can use the equation (5) as follows:

$$\left.\begin{aligned} f_1(x,y,z) &= x \\ f_2(x,y,z) &= y \\ f_3(x,y,z) &= z \end{aligned}\right\} \quad (6)$$

where, $f_1 = \alpha\, x(1-x) - \beta\, x\, y$, $f_2 = \gamma\, xy(x-z)$, $f_3 = \rho\, y\, z$. Here are five equilibrium points found in Equation (5):

$$\left.\begin{aligned} EP_1 &= (0,0,0) \\ EP_2 &= (\tfrac{\alpha-1}{\alpha},0,0) \\ EP_3 &= (-\tfrac{1}{\sqrt{\gamma}}, \tfrac{-1+\alpha+\frac{\alpha}{\sqrt{\gamma}}}{\beta},0) \\ EP_4 &= (\tfrac{1}{\sqrt{\gamma}}, \tfrac{-1+\alpha+\frac{\alpha}{\sqrt{\gamma}}}{\beta},0) \\ EP_5 &= (\tfrac{-\beta-\rho+\alpha\rho}{\alpha\rho}, \tfrac{1}{\rho}, \tfrac{-\beta^2\gamma-2\beta\gamma\rho+\alpha\beta\gamma\rho+\alpha^2\rho^2-\gamma\rho^2+2\alpha\gamma\rho^2}{\alpha\gamma\rho(\beta+\rho-\alpha\rho)}) \end{aligned}\right\} \quad (7)$$

Equation (5) has an equilibrium point defined as $EP_j (j = 1, ..., 5)$. To analyze linear stability, construct a Taylor series from equation (5):

$$\begin{pmatrix} x_{j+1} \\ y_{j+1} \\ z_{j+1} \end{pmatrix} = \begin{pmatrix} \frac{\partial f_1}{\partial \check{x}} & \frac{\partial f_1}{\partial \check{y}} & \frac{\partial f_1}{\partial \check{z}} \\ \frac{\partial f_2}{\partial \check{x}} & \frac{\partial f_2}{\partial \check{y}} & \frac{\partial f_2}{\partial \check{z}} \\ \frac{\partial f_3}{\partial \check{x}} & \frac{\partial f_3}{\partial \check{y}} & \frac{\partial f_3}{\partial \check{z}} \end{pmatrix}_{(p*,\bar{y},\bar{z})} \begin{pmatrix} x_t \\ y_t \\ z_t \end{pmatrix}$$

Equations (8) and (9) provide the following results:

$$\begin{aligned} \left.\frac{\partial f_1}{\partial x}\right|_{EP_j} &= (1-\check{x})\alpha - \check{x}\alpha - \check{y}\beta, \\ \left.\frac{\partial f_1}{\partial y}\right|_{EP_j} &= -\beta\,\check{x}, \qquad \left.\frac{\partial f_1}{\partial z}\right|_{EP_j} = 0, \\ \left.\frac{\partial f_2}{\partial x}\right|_{EP_j} &= \check{x}\check{y}\gamma + \check{y}(\check{x}-\check{z})\gamma, \\ \left.\frac{\partial f_2}{\partial y}\right|_{EP_j} &= \check{x}(\check{x}-\check{z})\gamma, \\ \left.\frac{\partial f_2}{\partial z}\right|_{EP_j} &= -\check{x}\check{y}\gamma, \\ \left.\frac{\partial f_3}{\partial x}\right|_{EP_j} &= 0, \\ \left.\frac{\partial f_3}{\partial y}\right|_{EP_j} &= \rho\,\check{z}, \qquad \left.\frac{\partial f_3}{\partial z}\right|_{EP_j} = \rho\,\check{y}. \end{aligned}$$

Consider the matrix:

$$J = \begin{pmatrix} u_{11} & u_{12} & u_{13} \\ u_{21} & u_{22} & u_{23} \\ u_{31} & u_{32} & u_{33} \end{pmatrix}$$

$$u_{11} = \tfrac{\partial f_1}{\partial x}|_{EP_j},\ u_{12} = \tfrac{\partial f_1}{\partial y}|_{EP_j},\ u_{13} = \tfrac{\partial f_1}{\partial z}|_{EP_j}$$

$$u_{21} = \tfrac{\partial f_2}{\partial x}|_{EP_j},\ u_{22} = \tfrac{\partial f_2}{\partial y}|_{EP_j},\ u_{23} = \tfrac{\partial f_2}{\partial z}|_{EP_j}$$

$$u_{31} = \tfrac{\partial f_3}{\partial x}|_{EP_j},\ u_{32} = \tfrac{\partial f_3}{\partial y}|_{EP_j},\ u_{33} = \tfrac{\partial f_3}{\partial z}|_{EP_j}$$

The characteristic equation is:

$$det\begin{pmatrix} u_{11}-\varsigma & u_{12} & u_{13} \\ u_{21} & u_{22}-\varsigma & u_{23} \\ u_{31} & u_{32} & u_{33}-\varsigma \end{pmatrix} = 0$$

The following could be substituted for it:

$$\varsigma^3 + m_1\varsigma^2 + m_2\varsigma + m_3 = 0$$

where

$$m_1 = -(u_{11}+u_{22}+u_{33}),$$
$$m_2 = u_{11}u_{22} - u_{12}u_{21} + u_{11}u_{33} - u_{13}u_{31} + u_{22}u_{33} - u_{23}u_{32},$$
$$m_3 = -u_{11}u_{22}u_{33} + u_{11}u_{23}u_{32} + u_{12}u_{21}u_{33} - u_{12}u_{23}u_{31} - u_{13}u_{21}u_{32} + u_{13}u_{22}u_{31}.$$

Definition 1. (Guckenheimer and Holmes 1983; Strogatz 2015): Let an equilibrium point of a three-dimensional system have eigenvalues λ_1, λ_2, and λ_3. Its local stability is defined as follows:

i. *Stable*: All eigenvalues have negative real parts, $\mathrm{Re}(\lambda_1) < 0$, $\mathrm{Re}(\lambda_2) < 0$, and $\mathrm{Re}(\lambda_3) < 0$, so trajectories approach the equilibrium.

ii. *Source*: At least one eigenvalue has a positive real part, $\mathrm{Re}(\lambda_i) > 0$ for some $i \in \{1,2,3\}$, making the equilibrium locally unstable.

iii. *Unstable spiral*: Complex eigenvalues with positive real parts cause trajectories to spiral away from the equilibrium.

iv. *Saddle point*: Eigenvalues have mixed signs of real parts; some positive and some negative, resulting in stability along certain directions and instability along others.

v. *Non-hyperbolic*: Any eigenvalue has zero real part, so linearization alone is insufficient to determine stability.

To determine the types of the five equilibrium points, we can compute their eigenvalues by using parameter values of $\alpha = 2.85$, $\beta = 3.14$, $\rho = 2.54$ and γ=6.85.

(i) The eigenvalues of EP_1 indicate that it is a source point:

$$\Lambda_{11} = 2.85, \qquad \Lambda_{12} = \Lambda_{13} = 0.$$

(ii) The equilibrium point EP_2 is a saddle point, since

$$\Lambda_{21} = 2.88632, \qquad \Lambda_{22} = -0.85, \qquad \Lambda_{23} = 0.$$

(iii) The point EP_3 is an unstable spiral (source) with eigenvalues

$$\Lambda_{31} = 1.54446 + 2.3625\iota,$$
$$\Lambda_{32} = 1.54446 - 2.3625\iota,$$
$$\Lambda_{33} = 2.37735.$$

(iv) The equilibrium point EP_4 exhibits unstable spiral (source) behavior:

$$\Lambda_{41} = 0.455535 - 1.10711\iota,$$
$$\Lambda_{42} = 0.455535 + 1.10711\iota,$$
$$\Lambda_{43} = 0.615643.$$

(v) The eigenvalues at EP_5 show that it is an unstable point:

$$\Lambda_{51} = 1.33214,$$
$$\Lambda_{52} = 0.527041 + 1.01841\iota,$$
$$\Lambda_{53} = 0.527041 - 1.01841\iota.$$

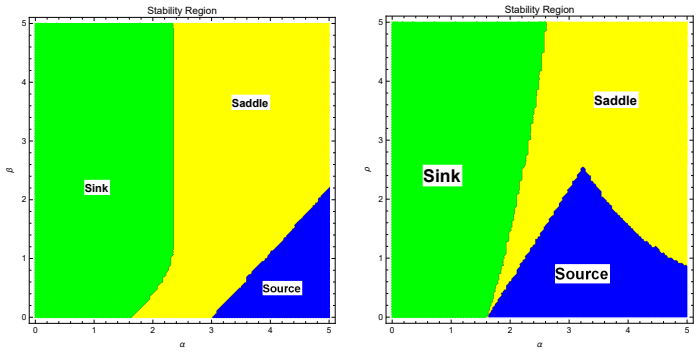

(a) Topological classification of EP_5 for (α,β) at $\gamma = 6.85, \rho = 2.54$, $\alpha \in [0,5], \beta \in [0,5]$.

(b) Topological classification of EP_5 for (α,ρ) at $\gamma = 6.85, \beta = 3.14$, $\alpha \in [0,5], \rho \in [0,5]$.

Figure 2 Topological classification of EP_5 under different parameter planes.

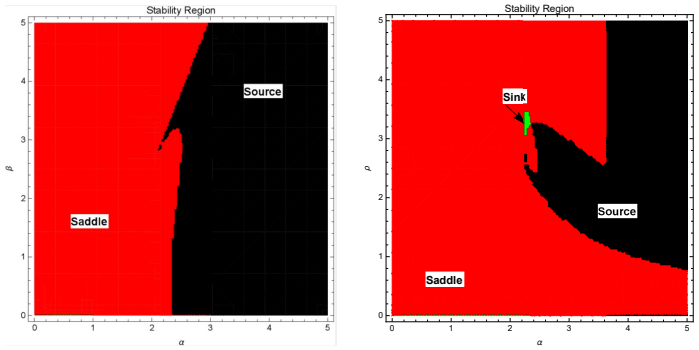

(a) Topological classification of EP_4 for (α,β) at $\gamma = 6.85, \rho = 2.54$, $\alpha \in [0,5], \beta \in [0,5]$.

(b) Topological classification of EP_4 for (α,ρ) at $\gamma = 6.85, \beta = 3.14$, $\alpha \in [0,5], \rho \in [0,5]$.

Figure 3 Topological classification of EP_4 under different parameter planes.

Based on the topological classification of EP_4 and EP_5, Figures (2*a*, 2*b*, 3*a*, 3*b*) illustrate their distinct characteristics of stability and dynamics within the system (5). A detailed equilibrium analysis is used to make recommendations for improving system performance in (Alarifi 2012). In a parametric analysis, the five equilibrium states ($EP_1, EP_2, EP_3, EP_4, EP_5$) are determined to be stable or unstable. The goal of our analysis is to examine the dynamics of the system's interactions based on its predation intensity. Dynamic behavior is influenced by the parameter γ in this system. Variations in the parameters α, β, γ, and ρ are performed to study the system's response in detail.

TRANSCRITICAL BIFURCATION ANALYSIS AT EP_2

At $\mathrm{EP}_2 = \left(x^* = \frac{\alpha-1}{\alpha},\ 0,\ 0\right)$, the bifurcation indicator is $\lambda_2 = \gamma(x^*)^2$. For $\alpha = 2.85$:

$$x^* = \frac{1.85}{2.85} \approx 0.6491, \quad (x^*)^2 \approx 0.4213$$

Thus, $\lambda_2 = \gamma \cdot 0.4213$. The bifurcation occurs at $\lambda_2 = 1$:

$$\gamma_c = \frac{1}{0.4213} \approx 2.374$$

Table 2 Values of λ_2 at EP_2 for varying γ, showing the flip bifurcation at $\gamma = 2.374$.

γ	x^*	$(x^*)^2$	$\lambda_2 = \gamma(x^*)^2$	**Remark**
1.0	0.6491	0.4213	0.4213	Stable
1.5	0.6491	0.4213	0.6320	Stable
2.0	0.6491	0.4213	0.8426	Approaching bifurcation
2.374	0.6491	0.4213	**1.0000**	Bifurcation occurs
3.0	0.6491	0.4213	1.2638	Unstable
4.0	0.6491	0.4213	1.6852	Strongly unstable
5.0	0.6491	0.4213	2.1065	Strongly unstable

A transcritical bifurcation occurs at $\gamma_c \approx 2.374$. For $\gamma < \gamma_c$, $y^* = 0$ is stable; for $\gamma > \gamma_c$, $y^* > 0$ invades and EP_2 loses stability. See Fig. 4.

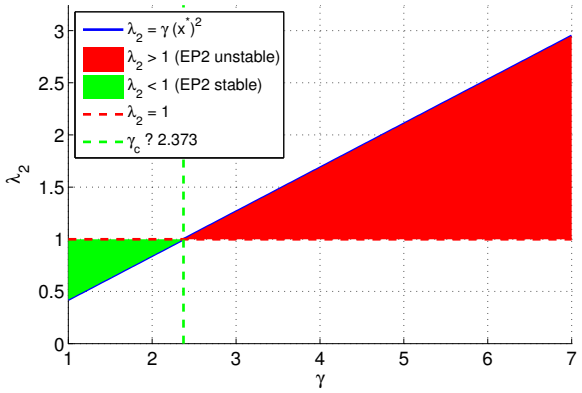

Figure 4 Bifurcation diagram of λ_2 vs γ at EP_2.

ANALYZE NEIMARK-SACKER BIFURCATION AT EP_5

When a key system parameter reaches a critical value, the Neimark-Sacker bifurcation occurs, leading to a shift from stability to the emergence of periodic orbits. In our study, we consider the interaction strength γ between species x and y as the bifurcation parameter to induce and analyze this bifurcation. We investigate the local behavior around the unstable equilibrium point, specifically to substantiate the presence of the NS bifurcation at EP_5.

The characteristic equation at

$$EP_5 = \left(\frac{-\beta-\rho+\alpha\rho}{\alpha\rho},\ \frac{1}{\rho},\ \frac{-\beta^2\gamma - 2\beta\gamma\rho + \alpha\beta\gamma\rho + \alpha^2\rho^2 - \gamma\rho^2 + 2\alpha\gamma\rho^2}{\alpha\gamma\rho(\beta+\rho-\alpha\rho)}\right)$$

is

$$\lambda^3 + m_1\lambda^2 + m_2\lambda + m_3 = 0.$$

where

$$\left.\begin{aligned} m_1 &= -(\alpha+\gamma+\rho), \\ m_2 &= \alpha\gamma + \alpha\rho + \gamma\rho + \beta, \\ m_3 &= -\alpha\beta\gamma - \alpha\beta\rho - \alpha\gamma\rho - \beta\rho - \rho^2. \end{aligned}\right\}$$

EP_5 is local asymptotically stable if m_1, m_2 and m_3 satisfy the Hurwitz (1895) stability criteria, i.e., $m_1 > 0, m_3 > 0$ and $m_1 m_2 - m_3 > 0$.

Theorem: The system exhibits a Neimark-Sacker (NS) bifurcation at equilibrium EP_5 when the interaction strength γ crosses the critical value γ_0, provided the following conditions hold:

$$m_1(\gamma_0) > 0, \quad m_3(\gamma_0) > 0, \quad m_1 m_2 - m_3 = 0, \quad (m_1 m_2)' \neq m_3'.$$

Proof. We take γ as the bifurcation parameter. The critical value γ_0 satisfies

$$m_1(\gamma_0)m_2(\gamma_0) - m_3(\gamma_0) = 0.$$

The characteristic equation at EP_5 becomes

$$\lambda^3 + m_1\lambda^2 + m_2\lambda + m_3 = 0 \quad \Rightarrow \quad (\lambda^2 + m_2)(\lambda + m_1) = 0$$

yielding roots $-m_1$ and $\pm i\sqrt{m_2}$. A pair of purely imaginary roots and one negative real root indicate a Hopf-like scenario, thus satisfying a necessary condition for NS bifurcation.

To confirm the bifurcation, the transversality condition must be met:

$$\frac{d}{d\gamma}\Re(\lambda(\gamma))\Big|_{\gamma=\gamma_0} \neq 0.$$

We express eigenvalues as $\lambda_{1,2} = \phi(\gamma) \pm i\psi(\gamma)$, $\lambda_3 = -m_1$. Differentiating the characteristic equation implicitly and evaluating at $\gamma = \gamma_0$ (where $\phi(\gamma_0) = 0$, $\psi(\gamma_0) = \sqrt{m_2(\gamma_0)}$), yields

$$\phi'(\gamma_0) = \frac{1}{2} \cdot \frac{m_3 - (m_1 m_2)'}{m_1^2 + m_2}.$$

Thus, the NS bifurcation occurs if $(m_1 m_2)' \neq m_3'$.

From numerical simulations, the bifurcation appears at $\gamma_0 = 4.77788$, near the equilibrium $(0.301002, 0.282486, -0.394335)$. □

NUMERICAL ANALYSIS

A systematic exploration of various parametric regimes was conducted to assess their impact on the system's dynamical behavior. This analysis facilitated a comprehensive understanding of the conditions under which chaotic dynamics emerge. In Figure 5, bifurcation diagrams for species x, y, and z are presented with fixed parameters $\alpha = 2.85$, $\beta = 3.14$, and $\rho = 2.54$, while the parameter γ is varied over the interval $[5, 7]$. Similarly, Figure 6 illustrates bifurcation diagrams for the same species under $\alpha = 2.74$, $\beta = 3.24$, and $\rho = 3.54$, with γ ranging from 1 to 7. Furthermore, evidence of a Neimark–Sacker bifurcation is apparent in Figures 6b and 6c, characterized by a period-doubling of the invariant curves.

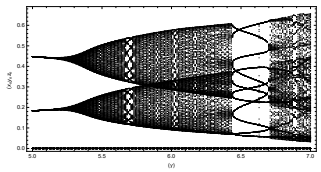

(a) 3D phase projection of prey (x), intermediate predator (y), and top predator (z).

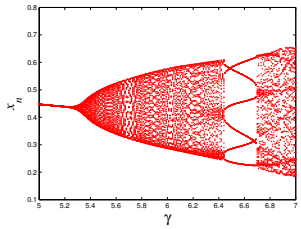

(b) NS Bifurcation diagram of prey population (x) as γ increases.

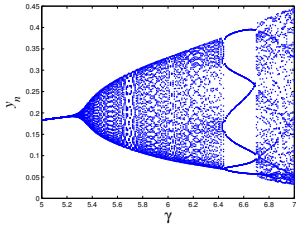

(c) NS Bifurcation diagram of intermediate predator (y) responding to prey and top predator variations.

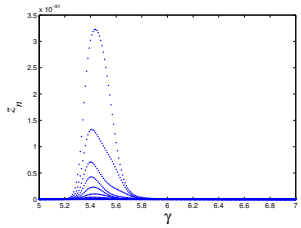

(d) NS Bifurcation diagram of top predator (z), reflecting higher trophic-level sensitivity.

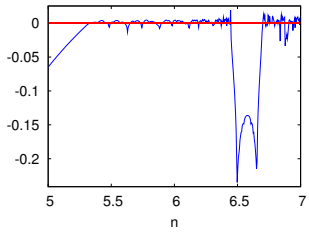

(e) Maximum Lyapunov exponent (MLE), indicating transitions from stable to chaotic behavior.

Figure 5 Neimark Sacker Bifurcation structure and dynamical transitions in a three-species food chain model for fixed parameters $\alpha = 2.85$, $\beta = 3.14$, and $\rho = 2.54$, as γ increases from 5 to 7. 5a illustrates the system's overall trajectory in 3D phase space; 5b, 5c, 5d show the bifurcation patterns of prey, intermediate predator, and top predator, respectively; 5e presents the MLE curve, confirming the onset of complex and chaotic dynamics in the trophic interactions.

To gain deeper insights into the system's dynamical characteristics, phase portraits were compared with their corresponding time series under varying initial conditions and parametric values, as detailed in Tables 3 and 4. The analyses reveal that the system exhibits diverse behaviors, including quasi-periodic motion, chaotic attractors, stable limit cycles, and stable periodic orbits.

STABILIZING THREE-SPECIES INTERACTIONS

By enhancing the OGY method, a stable period-1 orbit can be achieved for the three-species food chain model. Parameter γ is adjusted with time-dependent perturbations. When the unstable point approaches period-1 orbits, the control parameter can be modified due to the instability in the orbit. Thus, system (5) can be rewritten as follows to maintain controllability:

$$M_{j+1} = f_2(M_j, \omega) \tag{15}$$

Table 3 Comparison of phase portraits with corresponding time-series behavior

S.No	Initial conditions	Parametes	Dynamical Behavior
i	x_0=0.05 y_0=0.02 z_0=0.04	α=3.03 β=1.89 ρ=3.08 γ=5.75	Stable periodic
	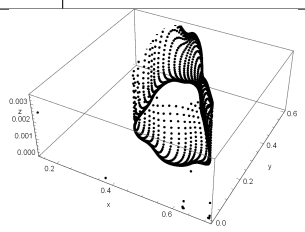	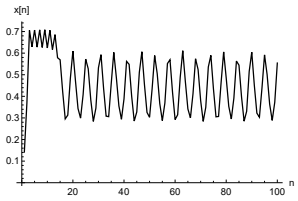	
ii	x_0=0.3 y_0=0.2 z_0=0.1	α=3.35 β=2.09 ρ=2.79 γ=5.02	Stable periodic
	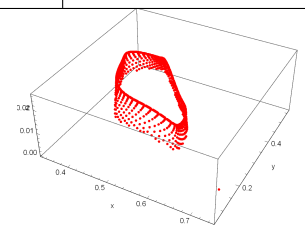	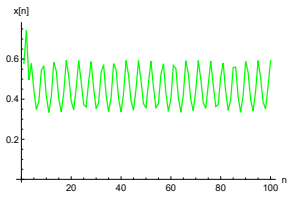	
iii	x_0=0.4 y_0=0.3 z_0=0.2	α=2.75 β=2.89 ρ=2.43 γ=5.85	Chaotic
	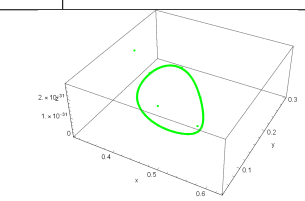	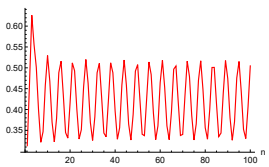	
iv	x_0=0.6 y_0=0.4 z_0=0.2	α=3.1 β=2.2 ρ=1.03 γ=6.05	Quasi-periodic
	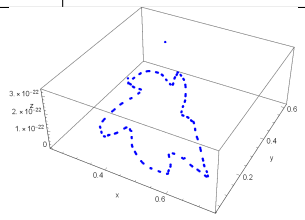	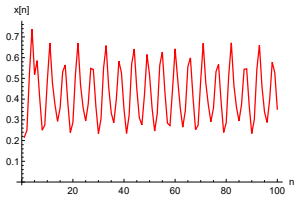	
v	x_0=0.03 y_0=0.02 z_0=0.01	α=2.95 β=3.09 ρ=2.73 γ=6.85	Chaotic
	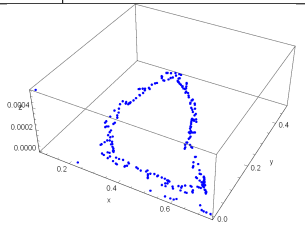	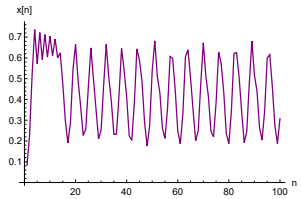	

Table 4 Comparison of phase portraits with corresponding time-series behavior

S.No	Initial conditions	Parametes	Dynamical Behavior
vi	x_0=0.05 y_0=0.02 z_0=0.04	α=3.03 β=1.89 ρ=3.08 γ=5.75	Chaotic
	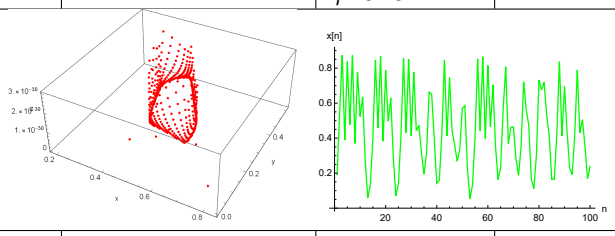		
vii	x_0=0.3 y_0=0.2 z_0=0.1	α=3.35 β=2.09 ρ=2.79 γ=5.02	Chaotic
	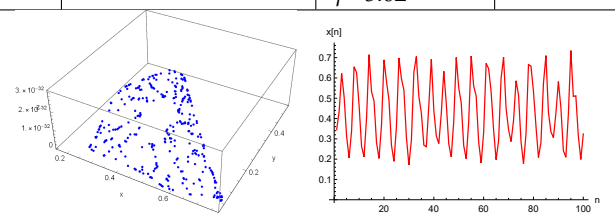		
viii	x_0=0.4 y_0=0.3 z_0=0.2	α=2.75 β=2.89 ρ=2.43 γ=5.85	Chaotic
	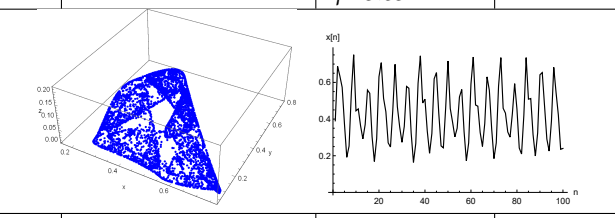		
ix	x_0=0.6 y_0=0.4 z_0=0.2	α=3.1 β=2.2 ρ=1.03 γ=6.05	Stable limit cycle
	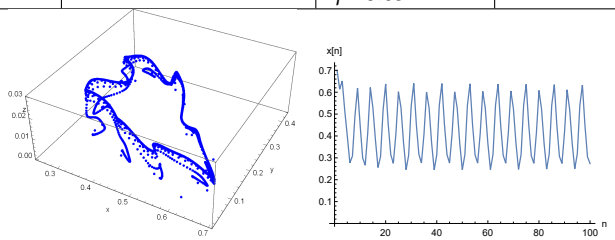		
x	x_0=0.4 y_0=0.2 z_0=0.3	α=2.93 β=1.79 ρ=3.23 γ=5.85	Stable periodic
	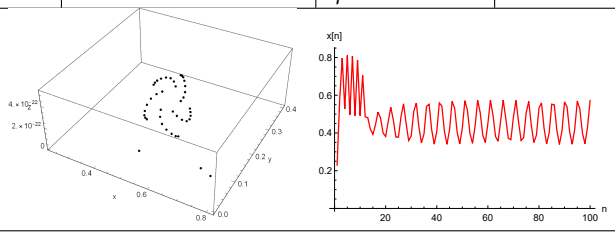		

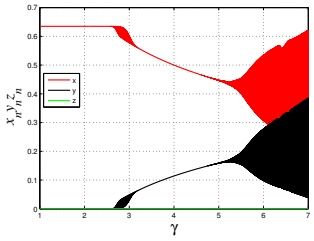

(a) 3D phase projection of prey (x), intermediate predator (y), and top predator (z), illustrating overall system dynamics.

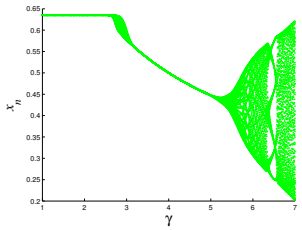

(b) Transcritical Bifurcation diagram of prey population (x) as γ increases.

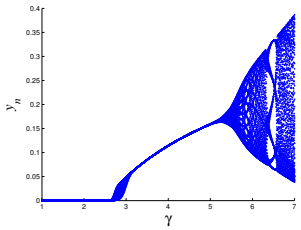

(c) Transcritical Bifurcation diagram of intermediate predator (y), reflecting changes in response to prey and top predator dynamics.

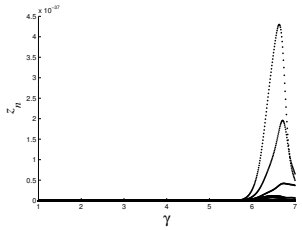

(d) Transcritical Bifurcation diagram of top predator (z), showing high sensitivity to lower trophic level fluctuations.

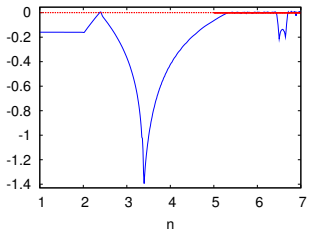

(e) Maximum Lyapunov exponent (MLE) versus γ, indicating stability, bifurcations, and chaotic regimes in the food chain model.

Figure 6 Transcritical bifurcation and dynamical transitions in a three-species food chain model for fixed parameters $\alpha = 2.74$, $\beta = 3.24$, and $\rho = 3.54$, as the bifurcation parameter γ is varied from 1 to 7. Subfigures 6a, 6b, 6c, 6d illustrate population-level responses for prey, intermediate predator, and top predator, showing characteristic features of transcritical bifurcation across trophic levels, while 6e depicts the corresponding MLE indicating transitions between stable and chaotic regimes.

where $M_j \in \Re^3$, and f_2 is a nonlinear vector function with $\omega \in \Re$ as a bifurcation parameter. When f_2 is sufficiently smooth and ω can be externally adjusted, for $\mid \omega - \bar{\omega} \mid < \delta$, the system meets the requirement at some point, with $\bar{\omega}$ being the rated value. Consider ω as a variable parameter near $\bar{\omega} = 6.9$. Consequently, for system (5), the equilibrium point EP_5 is found to be $(0.215361, 0.393701, -0.462502)$ with parameters $\alpha = 2.85$, $\beta = 3.14$, $\gamma = 6.85$, and $\rho = 2.54$. To achieve a periodic orbit, initial conditions must lie within the chaotic attractor. Because of the chaotic behavior, we can use feedback control to guide the path to a nearby unstable periodic orbit.

Equation (15) can be expressed using the Taylor expansion around the unstable point EP_5, denoted as $M^*(\bar{\omega})$.

$$M_{j+1} - M^*(\bar{\omega}) = \tilde{V}(M_j - M^*(\bar{\omega})) + \tilde{B}(\omega - \bar{\omega}) \tag{16}$$

Here, $\tilde{V}$ is the derivative matrix of f_2 with respect to the variables (x, y, z), represented by $p*$.

$$\tilde{V} = D_{p*} f_2(p*, \omega)$$

$$\tilde{V} = \begin{pmatrix} \alpha\,(1-x) - x\,\alpha - y\,\beta & -\beta x & 0 \\ \gamma\,x\,y + y\,(x-z)\,\gamma & x\,(x-z)\,\gamma & -x\,y\,\gamma \\ 0 & \rho\,z & -\rho\,y \end{pmatrix} \tag{17}$$

The derivative matrix of $f_2(M, \gamma)$ with respect to the variable γ is denoted as $\tilde{B}$.

$$\tilde{B} = D_{\gamma} f_2(p*, \gamma)$$

$$\tilde{B} = \begin{pmatrix} 0 \\ x\,y\,(x-z) \\ 0 \end{pmatrix} \tag{18}$$

The parameters $\alpha = 2.85$, $\beta = 3.14$, γ=6.85, $\rho = 2.54$, and the fixed point $EP_5(0.215361, 0.393701, -0.462502)$ should be entered into the matrices $\tilde{V}$ and $\tilde{B}$:

$$\tilde{V} = \begin{pmatrix} 0.38622 & -0.676234 & 0 \\ 2.40889 & 1 & -0.580797 \\ 0 & -1.17475 & 1 \end{pmatrix} \tag{19}$$

$$\tilde{B} = \begin{pmatrix} 0 \\ 0.0574746 \\ 0 \end{pmatrix}$$

ω is a time-dependent parameter that follows a linear function:

$$\omega - \bar{\omega} = -\tilde{H}^T\,(M_j - M^*(\bar{\omega})) \tag{20}$$

Then, (11) implies

$$M_{j+1} - M^*(\bar{\omega}) = (\tilde{V} - \tilde{H}^T\tilde{B})\,(M_j - M^*(\bar{\omega})) \tag{21}$$

In the case of a stable fixed point $M^*(\bar{\omega})$, the eigenvalues of $\tilde{V} - \tilde{H}^T\tilde{B}$ must be within the unit disc. Use Volterra (1962) to find a controlled matrix

$$\tilde{S} = \begin{pmatrix} \tilde{B} & \tilde{V}\tilde{B} & \tilde{A}^2\tilde{B} \end{pmatrix}$$

$$\tilde{S} = \begin{pmatrix} 0 & -0.0388663 & 0.0262827 \\ 0.057475 & 0.0574746 & 0.0574746 \\ 0 & -0.0675185 & 0.0793176 \end{pmatrix} \tag{22}$$

The stabilization of chaos is achieved using the matrix $\tilde{H}^T$, where

$$\tilde{H}^T = \begin{pmatrix} e_3 - \omega_3 & e_2 - \omega_2 & e_1 - \omega_1 \end{pmatrix} T^{-1}$$

and

$$T = \tilde{S}\tilde{G}$$

$$\tilde{G} = \begin{pmatrix} \omega_2 & \omega_1 & 0 \\ \omega_1 & 1 & 0 \\ 1 & 0 & 0 \end{pmatrix} \tag{23}$$

$\omega_j (j = 1, 2, 3)$ are the coefficients of matrix V. That is

$$|\,\Lambda I - \tilde{V}\,| = \Lambda^3 + \omega_1\,\Lambda^2 + \omega_2\,\Lambda + \omega_3 \tag{24}$$

From equation (17) and (24), we get;

$$|\,\Lambda I - \tilde{V}\,| = \begin{vmatrix} \Lambda - 0.38622 & 0.676234 & 0 \\ -2.40889 & \Lambda - 1 & 0.580797 \\ 0 & 1.17475 & \Lambda - 1 \end{vmatrix}$$

$$= -\Lambda^3 + 2.38622\,\Lambda^2 - 2.71912\,\Lambda + 1.75168 \tag{25}$$

therefore, $\omega_1 = 2.38622$, $\omega_2 = -2.71912$ and $\omega_3 = 1.75168$.

Let e_1, e_2, e_3 denote the coefficients of the characteristic polynomial of $(\tilde{V} - \tilde{B}\tilde{H}^T)$. Then

$$|\,\mu\,I - (\tilde{V} - \tilde{B}\tilde{H}^T)\,| = \mu^3 + e_1\,\mu^2 + e_2\,\mu + e_3 \tag{26}$$

$$T = \tilde{S}\tilde{G} = \begin{pmatrix} 0 & -0.0388663 & 0.0262827 \\ 0.057475 & 0.0574746 & 0.0574746 \\ 0 & -0.0675185 & 0.0793176 \end{pmatrix} \begin{pmatrix} -2.71912 & 2.38622 & 1 \\ 2.38622 & 1 & 0 \\ 1 & 0 & 0 \end{pmatrix}$$

$$T = \begin{pmatrix} -0.0664608 & -0.0388663 & 0 \\ 0.0383412 & 0.194622 & 0.0574746 \\ 0.0817964 & -0.0675185 & 0 \end{pmatrix} \tag{27}$$

$$T^{-1} = \begin{pmatrix} -51.6113 & -8.88178 \times 10^{-16} & 29.7095 \\ 62.5253 & 0 & 50.8028 \\ -177.295 & 17.399 & 152.21 \end{pmatrix} \tag{28}$$

At $EP_5(0.215361, 0.393701, -0.462502)$, $\tilde{V}$ has eigenvalues:

$$e_\mu = 1.33214$$

$$e_{1\mu} = 0.527041 + 1.01841\iota$$

$$e_{2\mu} = 0.527041 - 1.01841\iota$$

The eigenvalues ψ_1, ψ_2, ψ_3 of the matrix $(\tilde{V} - \tilde{B}\tilde{H}^T)$ refer as adjustment values.

$$\left|\mu I - (\tilde{V} - \tilde{B}\tilde{H}^T)\right| = \mu^3 - (\psi_1 + \psi_2 + \psi_3)\,\mu^2 + (\psi_1\psi_2 + \psi_2\psi_3 + \psi_3\psi_1)\,\mu - \psi_1\psi_2\psi_3. \tag{29}$$

Following are the correlations between coefficients and roots:

$$\begin{aligned} e_1 &= -(\psi_1 + \psi_2 + \psi_3), \\ e_2 &= \psi_1\psi_2 + \psi_2\psi_3 + \psi_3\psi_1, \\ e_3 &= -\psi_1\psi_2\psi_3. \end{aligned}$$

From equation (22), we deduce that $\tilde{H}^T$ is not unique. Suppose $(e_1, e_2, e_3) = (-|e_\mu|, -|e_\mu|, 0)$.

$$\tilde{H}^T = \begin{pmatrix} 0 - \omega_3 & -|e_\mu| - \omega_2 & -|e_\mu| - \omega_1 \end{pmatrix} T^{-1}$$

$$\tilde{H}^T = \begin{pmatrix} -1.75168 & 1.38698 & 3.71836 \end{pmatrix} \begin{pmatrix} -51.6113 & -8.88178 \times 10^{-16} & 29.7095 \\ 62.5253 & 0 & 50.8028 \\ -177.295 & 17.399 & 152.21 \end{pmatrix}$$

$$\tilde{H}^T = \begin{pmatrix} 836.373 & -64.6957 & -688.476 \end{pmatrix} \tag{30}$$

Once $\tilde{H}^T$ is established, Equation (16) allows us to compute $\left|\tilde{H}^T(M_j - M^*(\bar{\omega}))\right| < \sigma$. This condition defines a region with a width given by:

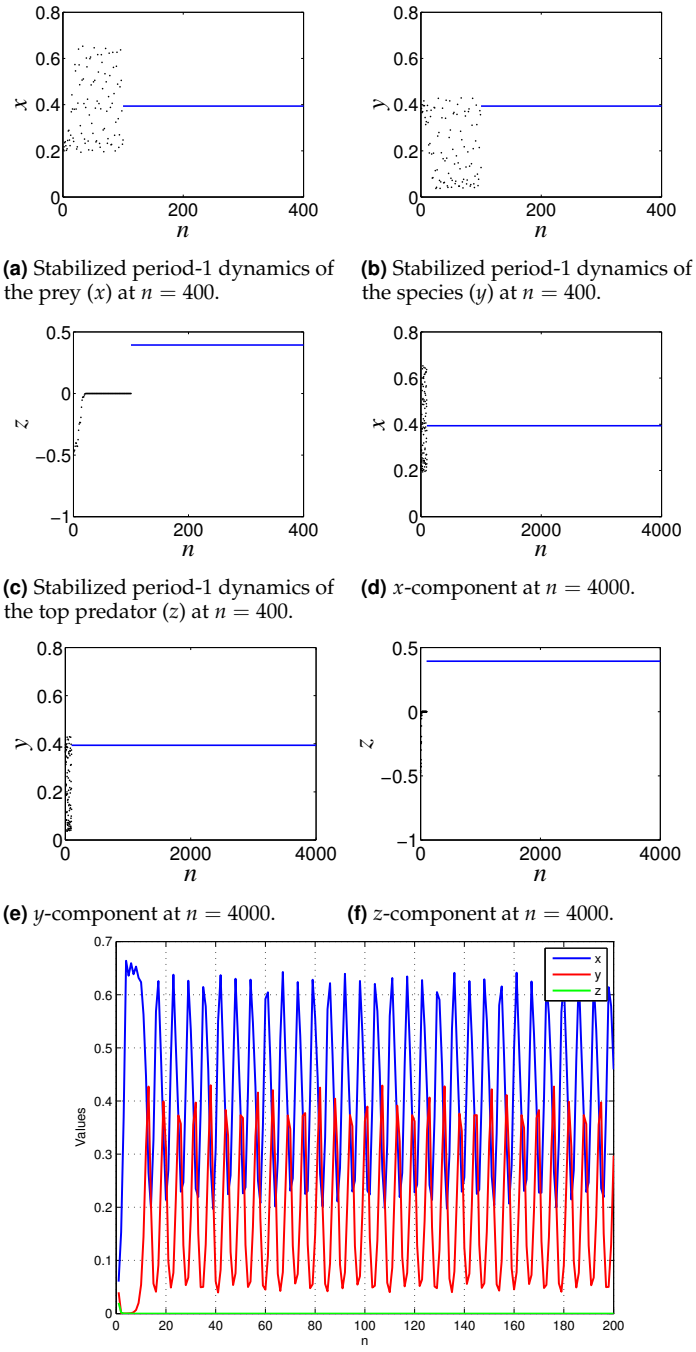

(a) Stabilized period-1 dynamics of the prey (x) at $n = 400$.

(b) Stabilized period-1 dynamics of the species (y) at $n = 400$.

(c) Stabilized period-1 dynamics of the top predator (z) at $n = 400$.

(d) x-component at $n = 4000$.

(e) y-component at $n = 4000$.

(f) z-component at $n = 4000$.

(g) Time series of state variables

Figure 7 Evolution of the system's state variables under FCM control showing periodic behavior corresponding to Cycle-1. Subfigures 7a, 7b, and 7c, show the x, y, and z-components, respectively, at iteration $n = 400$, while subfigures 7d, 7e, and 7f display the corresponding components at iteration $n = 4000$. Subfigure 7g presents the full time series of the state variables, illustrating the periodic dynamics.

$$\frac{2\sigma}{|\tilde{H}^T|}$$

Parameters can be controlled within this region if M_j lies within it; otherwise, control is not achievable. To determine the controlled rate, we can use the following formula:

$$\begin{aligned}\omega - \bar{\omega} = &-\tilde{H}^T\left(M_j - M^*(\bar{\omega})\right)\bar{u}(\bar{\omega}) \\ &\times \left(\sigma - \left|\tilde{H}^T(Z_j - Z^*(\bar{\omega}))\right|\right).\end{aligned} \tag{31}$$

where

$$\bar{u}(\bar{\omega}) = \begin{cases} 0, & \bar{\omega} < 0, \\ 1, & \bar{\omega} > 0. \end{cases}$$

Figure $(7a - 7f)$ illustrates that when $e_1 = 1.33214$, $e_2 = 1.33214$, and $e_3 = 0$, controlling chaotic motion to a period-1 orbit is feasible by selecting $n = 400$ or $n = 4000$.

CONCLUSION

This study investigates the dynamic responses of a discrete-time Food Chain Model (FCM) to predator pressure under stringent conditions, with a focus on the variety of equilibrium states that can arise within such systems. A Transcritical bifurcation is identified at the equilibrium point EP_2, while a NS bifurcation occurs at EP_4 when the bifurcation parameter γ is approximately 2.374 and 4.77788, respectively. The stabilization of a period-1 orbit is achieved through an enhanced OGY control method. Successive iterations employing different controller poles successfully stabilize the periodic orbit while preserving the intrinsic dynamics of the original system. Numerical simulations demonstrate the effectiveness of this control strategy and its broader implications. The model reveals species dynamics fluctuating between equilibrium states and chaotic behavior, driven by factors such as population size, birth rate, and survival rate. The theoretical insights derived from this work offer valuable perspectives for future research in biological and ecological systems. The application of OGY based chaos control proves effective in regulating complex system dynamics under parameter variation, emphasizing the relevance and potential of these approaches for further exploration and development.

Moreover, the OGY chaos control method demonstrates how chaotic population dynamics can be stabilized in the mathematical model. These results suggest that similar strategies could potentially be used to manage ecosystems by keeping populations within desirable limits, avoiding extreme fluctuations, and maintaining balance between species. Such insights provide guidance for developing sustainable approaches to pest management, biodiversity conservation, and the overall stability of ecological systems.

Acknowledgments

For the purposes of executing the research, no specific funding has been received.

Ethical standard

The authors have no relevant financial or non-financial interests to disclose.

Availability of data and material

Not applicable.

Conflicts of interest

The authors declare that there is no conflict of interest regarding the publication of this paper.

LITERATURE CITED

Abbas, A. and A. Khaliq, 2023 Analyzing predator-prey interaction in chaotic and bifurcating environments. Chaos Theory and Applications **5**: 207–218.

Abbas, A. and A. Khaliq, 2024 Chaotic dynamics in predator-prey interactions. Physica Scripta **99**: 055260.

Alarifi, E. A., 2012 Dynamical complexities in a discrete-time food chain. Computational Ecology and Software **2**: 124.

Alasty, A. and H. H. Salarieh, 2007 Nonlinear feedback control of chaotic pendulum in presence of saturation effect. Chaos, Solitons & Fractals **31**: 292–304.

Baydemir, P., H. Merdan, E. Karaoglu, and G. Sucu, 2020 Complex dynamics of a discrete-time prey-predator system with leslie type: Stability, bifurcation analyses and chaos. International Journal of Bifurcation and Chaos **30**: 2050149.

Chakraborty, K. and T. K. Kar, 2012 Optimal harvesting in a prey-predator fishery with stage structure and nonlinear controls. Biosystems **109**: 123–136.

Chen, L. and G. Chen, 2007 Controlling chaos in an economics model. Physica A **374**: 349–358.

Din, Q., 2017 Complexity and chaos control in a discrete-time prey-predator model. Communications in Nonlinear Science and Numerical Simulation **49**: 113–134.

Feng, G., 2020a Chaotic dynamics and chaos control of hassell-type recruitment population model. Discrete Dynamics in Nature and Society **2020**: 8148634.

Feng, G., 2020b Controlling chaos of the ricker population model. American Journal of Bioscience and Bioengineering **16**: 424–431.

Gomes, A. A., E. Manica, and M. C. Varriale, 2006 Applications of chaos control techniques to a three-species food chain. Chaos, Solitons & Fractals **36**: 1097–1107.

Guckenheimer, J. and P. Holmes, 1983 *Nonlinear Oscillations, Dynamical Systems, and Bifurcations of Vector Fields*. Springer, New York.

Hashemi, S., M. A. Pourmina, S. Mobayen, and M. R. Alagheband, 2020 Design of a secure communication system based on finite-time chaos synchronisation. International Journal of Systems Science **51**: 1969–1986.

Holyst, J. A. and K. Urbanowicz, 2000 Chaos control in economical model by time-delayed feedback control. Physica A **287**: 587–598.

Hurwitz, A., 1895 Ueber die bedingungen, unter welchen eine gleichung nur wurzeln mit negativen reellen teilen besitzt. Mathematische Annalen **46**: 273–284.

Ivanchikov, P. V. and L. V. Nedorezov, 2012 About a modification of may model of parasite-host system dynamics. Computational Ecology and Software **2**: 42–52.

Jiang, X. W., X. Y. Chen, T. W. Huang, and H. C. Yang, 2020 Bifurcation and control for a predator-prey system with two delays. IEEE Transactions on Circuits and Systems II **99**: 1.

Khan, M. A., J. Ghosh, and B. Sahoo, 2015 Controlling chaos in a food chain model through threshold harvesting. Fisheries and Aquaculture Journal **6**: 4.

Lotka, A. J., 1925 *Elements of Mathematical Biology*. Williams and Wilkins, Baltimore.

May, R. M., 1974 *Stability and Complexity in Model Ecosystems*. Princeton University Press.

Mobayen, S., K. V. Christos, S. Kaçar, U. Çavuşoğlu, and B. Vaseghi, 2018 A chaotic system with infinite equilibria on an exponential curve and its engineering application. International Journal of Bifurcation and Chaos **28**: 1850112.
Mobayen, S., J. Ma, G. Pujol-Vazquez, L. Acho, and Q. Zhu, 2019 Adaptive finite-time stabilization of chaotic flow with a single unstable node using nonlinear sliding mode. Iranian Journal of Science and Technology, Transactions of Electrical Engineering **43**: 339–347.
Ott, E., C. Grebogi, and J. A. Yorke, 1990 Controlling chaos. Physical Review Letters **64**: 1196–1199.
Paine, R. T., 1966 Food web complexity and species diversity. The American Naturalist **100**: 65–75.
Panday, P., N. Pal, S. Samanta, and J. Chattopadhyay, 2018 Stability and bifurcation analysis of a three-species food chain model with fear. International Journal of Bifurcation and Chaos **28**: 1850001.
Parshad, R. D., E. Quansah, U. R. K. Black, S. K. Tiwari, and N. Kumari, 2016 Long time dynamics of a three-species food chain model with allee effect in the top predator. Computers and Mathematics with Applications **71**: 503–528.
Pyragas, K., 1992 Continuous control of chaos by self-controlling feedback. Physics Letters A **170**: 421–428.
Pyragas, K., 1995 Control of chaos via extended delay feedback. Physics Letters A **206**: 323–330.
Romeiras, F. J., C. Grebogi, E. Ott, and W. P. Dayawansa, 1992 Controlling chaotic dynamical systems. Physica D **58**: 165–192.
Selvam, A. G. M., S. B. Jacob, and R. Dhineshbabu, 2020 Nonlinear dynamics in population systems. Journal of Physics: Conference Series **1543**: 012010.
Sen, M., M. Banerjee, and A. Morozov, 2012 Bifurcation analysis of a ratio-dependent prey-predator model with the allee effect. Ecological Complexity **11**: 12–27.
Skalski, G. T. and J. F. Gilliam, 2001 Functional responses with predator interference: Ecological implications. Ecology **82**: 1200–1206.
Strogatz, S. H., 2015 *Nonlinear Dynamics and Chaos*. Westview Press, second edition.
Vaseghi, B., S. Mobayen, S. S. Hashemi, and A. Fekih, 2020 Fast reaching finite time synchronization for chaotic systems with application in medical image encryption. IEEE Access **9**: 25911–25925.
Vaseghi, B., M. A. Pourmina, and S. Mobayen, 2017 Finite-time chaos synchronization and its application in wireless sensor networks. Transactions of the Institute of Measurement and Control **40**: 3788–3799.
Volterra, V., 1962 *Opere Matematiche: Memorie e Note*. Accademia Nazionale dei Lincei, Rome.
Zhang, C. H., X. P. Yan, and G. H. Cui, 2010 Hopf bifurcations in a predator-prey system with a discrete delay and a distributed delay. Nonlinear Analysis: Real World Applications **11**: 4141–4153.
Znegui, W., H. Gritli, and S. Belghith, 2020a Poincaré map for passive dynamic walking of the compass-gait biped model. Chaos, Solitons & Fractals **130**: 109436.
Znegui, W., H. Gritli, and S. Belghith, 2020b Stabilization of compass-gait biped robot by controlled poincaré map. Nonlinear Dynamics **101**: 1061–1091.
Znegui, W., H. Gritli, and S. Belghith, 2021 A new poincaré map for investigating compass-gait biped robot. Applied Mathematical Modelling **94**: 534–557.

How to cite this article: Abbas, A., and Khaliq, A. Dynamics, Stability, and Bifurcation in Discrete-Time Predator-Prey Model. *ADBA Computer Science*, 3(1), 26-36, 2026.